IET Microwaves, Antennas & Propagation

Research Article

IET Journals
The Institution of Engineering and Technology

60 GHz radio link characteristic studies in hallway environment using antipodal linear tapered slot antenna

ISSN 1751-8725
Received on 10th July 2014
Revised on 14th July 2015
Accepted on 15th August 2015
doi: 10.1049/iet-map.2014.0787
www.ietdl.org

Purva Shrivastava, Rama Rao Thipparaju ✉

Department of Telecommunication Engineering, RADMIC, SRM University, Chennai 603 203, India
✉ *E-mail: ramarao@ieee.org*

Abstract: Millimetre-wave (MmW) frequencies offer large bandwidth with which gigabit data rates can be easily achieved with simple radio architectures. At MmW frequencies, the short wavelength enables integration of the antenna on the same chip as the microwave monolithic integrated circuits. This research work emphasises on the design and development of antipodal linear tapered slot antenna (ALTSA) using substrate integrated waveguide (SIW) technique and its radio link characteristics at 60 GHz for wireless local area network and wireless personal area network applications. SIW feeding technique is used to eliminate the unwanted radiations from feed. The proposed antenna is designed and simulated using three-dimensional (3D) electromagnetic tools. Radio propagation is profoundly site specific and depends on frequency of operation, interference from surroundings and other dynamic factors. To predict signal strength, delay and achievable data rates, it is important to characterise the radio channel. The radio link study is carried out using ALTSA with radio frequency measurement equipment to measure and characterise propagation channels in narrow hallway environment at 60 GHz.

1 Introduction

The evolution of wireless communication with gigabit data rates (Gbps) has drove interest in use of the extra high frequency (EHF) bands. With the available bandwidth of 7 GHz, the unlicenced 60 GHz band (57–64 GHz) is of great interest for the new generation wireless local area network (WLAN) and wireless personal area networks (WPANs), which will allow multimedia downloads at ultra-high speed with data rate of 1 Gbps [1]. The 60 GHz band has been proposed for variety of commercial and defence applications including automotive radars, imaging and medical devices and for other potential applications such as fixed and mobile network backhaul, enhancing network paths, 60 GHz radio local area networks, eliminate reception problems for apartment dwellers and temporary service restoration. The 60 GHz band has been recognised by a number of administrations as being appropriate for short-range communications technologies, and there are indications that equipment to utilise this band is starting to become available. The propagation characteristics of the 60 GHz band are characterised by high levels of oxygen absorption and rain attenuation [2, 3]. Oxygen absorption and attenuation through walls facilitate efficient frequency re-use capability. This limits the range of communication systems using this band; however, it makes 60 GHz attractive for a variety of short-range communication applications [1, 4]. Resulting from short transmission distances, these communications are highly secure and virtually interference free operation. In addition to large bandwidth, millimetre-wave (MmW) enables integration of the whole transceiver inside a small chip due to the short wavelength (λ) of 5–7 mm.

However, at 60 GHz path loss (PL) is more severe than at 2 or 5 GHz and implementing a highly integrated transceiver in complementary metal–oxide semiconductor will be a challenging task. This higher free-space loss can be compensated by the use of antennas with more pattern directivity and adaptive antenna arrays. Recently, there has been a great deal of interest in antennas for MmW applications, as they are of low profile, light weighted and easy to integrate with other planar devices [4]. For the MmW-based WLAN and WPAN applications, the antenna should satisfy a few characteristics of high directivity to reach the maximum range, enough bandwidth for rich multimedia content, small size for portable use, narrow beamwidth and low side lobe levels (SLLs) [1, 4]. Microstrip antennas, reflector type antenna and tapered slot antenna (TSA) have been widely used to take advantage of their moderately high gain, wide separation bandwidth and relatively low SLLs. TSA is a popular choice for applications such as ground penetration surveillance, medical, imaging, security and numerous other wireless communication applications [5, 6]. Many designs for the taper have been proposed and developed by various researchers all over the world [7, 8]. One such type of antenna is antipodal linear TSA (ALTSA). ALTSA has been investigated widely in academic and industry focusing the ultra-wideband (UWB) and very high frequency range [8–11], hardly any work is present in the EHF range. Compared with the conventional TSA, antipodal geometry has been incorporated in which one of the flares is on the upper side of the antenna while the other is on the lower part. Antipodal geometry allows perfect impedance matching without any stubs on the printed circuit board (PCB) and better current distribution on the antenna surface [9].

Traditional planar transmission lines have suffered larger losses than waveguide at higher frequency. Substrate integrated waveguide (SIW) technology has been proposed for MmW circuits and has been investigated by researchers from various parts of the world in the past 15 years [12]. In this study, SIW is composed of two rows of metallised via-holes which are connected with two metal plates on the top and bottom sides. The mechanism on which SIW operates is very much similar to a rectangular waveguide. SIW technology inherits most of the advantages of the conventional metallic waveguides such as complete shielding, low loss ease of fabrication, high-quality factor and high power-handling capability [11–13]. In addition, broadband operation is achieved with the help of optimised overlap matching section and by using via-hole arrangement, electric field leakage is reduced and insertion characteristic is improved [9].

It has been reported that a reduced antenna width is associated with degradation in radiation pattern, which is a significant problem for the design of compact TSAs [10, 11]. TSAs with corrugation structure have been used to reduce TSA width without any significant degradation in the radiation pattern [10, 11]. In

applications such as MmW radar and communication systems using directional antenna, it is preferred that the antenna has a high front to back (F/B) ratio and directivity. Corrugation has been proven successful in TSA structures for F/B ratio, gain and beamwidth improvement [14, 15].

In microwave systems, transmission loss is principally accounted for by the free-space loss. However, in the MmW bands additional loss factors such as gaseous losses and rain in the transmission medium come into show. At 60 GHz, smaller wavelengths causes strong attenuation over the free space, oxygen absorption and severe attenuation by surroundings allow frequency reuse and user privacy [3]. For the next generation WLAN and WPAN at 60 GHz, radio link propagation characteristics in typical indoor environments with a realistic channel model will be very helpful for the better understanding of propagation mechanisms and effects [16]. Precise estimation of propagation loss offers improved planning and deployment of access points in indoor environments. Three-dimensional (3D) ray tracing software tool, Wireless InSite from REMCOM and radio frequency (RF) equipment from Keysight Technologies were utilised to analyse the propagation characteristics. Thus, this paper presents complete electromagnetic (EM) simulations, measurements and validation results of plain and corrugated ALTSA with radio link investigations using RF equipment in hallway scenarios of an indoor environment at 60 GHz for WLAN and WPAN applications.

2 Antenna requirements, architecture and design

One of the key question that needs to be answered before MmW devices can be produced profitably in large quantities is how to realise a low-cost low profile, light weight and efficient antenna with other parts of the transceiver [17]. However, there are some additional requirements due to 60 GHz propagation characteristics. As the PL is high at 60 GHz, high antenna gain is required to compensate channel loss and the maximum radiation should be directive toward the receiver to maximise the coupling between devices. Traditionally horn, reflector and lens antennas have been used in MmW devices. These antennas have high gain and efficiency but they are not suitable for low-cost commercial devices because they are expensive, heavy, bulky and cannot be integrated with solid-state devices [4]. Therefore, planar antenna with high gain, efficiency and end-fire pattern is required. Such high gain antennas also lead to better security as it minimises the amount of energy radiated away from the transmitter. For the aforementioned reasons, the TSA have been chosen as a strong candidate because of their compromise in terms of size and efficiency.

The ALTSA is designed on 0.381 mm RT/Duroid 5880 substrate with dielectric permittivity $\epsilon_r = 2.20$ and $\tan\delta = 0.0004$ utilising 3D-EM tool, Computer Simulation Technology Microwave Studio (CST MWS). Fig. 1 depicts the configuration of the proposed ALTSA with SIW feeding. On one side, the input track is flared to produce half of the linear TSA and on the other side of substrate the ground plane is flared in the opposite direction to form the overall balanced antipodal. One of the advantages of the antipodal geometry is that it does not need to layout any stubs on the PCB to achieve impedance matching. The input impedance of the ALTSA is high and that of the SIW is low which causes a mismatch. To solve this problem, the flares are designed in a way that they overlap each other. The SIW feeding structure has two periodic rows of metallised cylindrical vias connecting the upper and lower flares of ALTSA which acts as dielectric filled rectangular waveguide.

Typical length of tapered slot line must be 3λ–8λ to achieve the gain of 7–14 dB [15]. Several lengths were simulated to determine the optimal tradeoff between the antenna length and the resulting antenna gain and beamwidth. To achieve the maximum gain, length of tapered slot line is set to 4.5λ at 60 GHz. Table 1 provides parameters of SIW-based ALTSA. The performance of ALTSA depends on the thickness t and the dielectric permittivity ε_r of the substrate. Equation (1) defines the effective thickness of

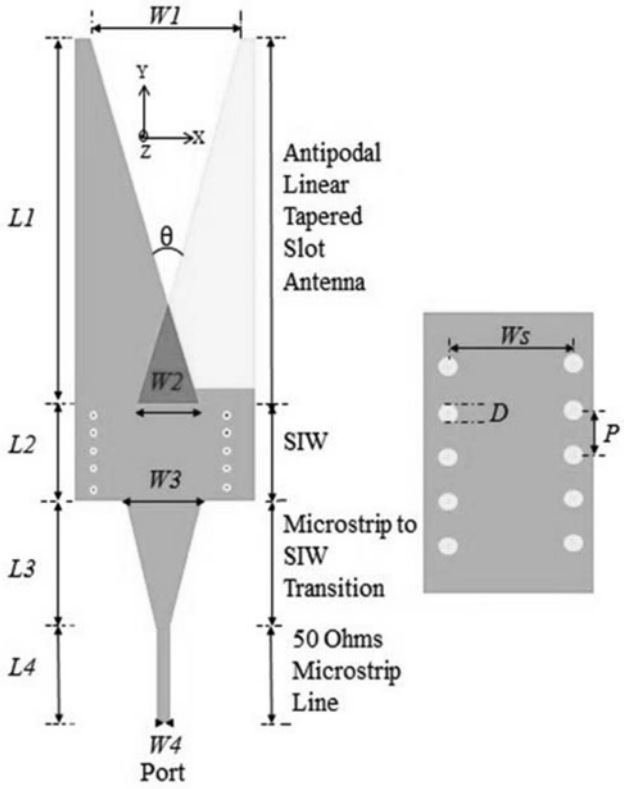

Fig. 1 *Proposed ALTSA design*

the substrate [18]

$$t_{\text{eff}} = t(\sqrt{\varepsilon_r - 1}) \tag{1}$$

For better performance effective thickness should lie within a range given by (2)

$$0.005 \leq \frac{t_{\text{eff}}}{\lambda} \leq 0.03 \tag{2}$$

When the distance between the via-holes are electrically small (<0.2λ), SIW can be replaced by a rectangular waveguide [12]. SIW can be commonly used as a transmission line which is similar to the rectangular waveguide in terms of mode and cut-off frequency properties. The effective width of the SIW structure W_s

Table 1 Dimension of ALTSA

Parameter	Dielectric substrate: RT/Duriod ($\epsilon_r = 2.20$, $h = 0.381$ mm)	
	Symbol	Value, mm
ALTSA length	L_1	22.35
SIW length	L_2	15
taper length	L_3	4.51
microstrip line length	L_4	2.75
ALTSA width	W_1	9.93
overlapping area width	W_2	1.8
taper width	W_3	3.12
microstrip line width	W_4	0.8
SIW width	W_{SIW}	6.2
diameter of vias	D	0.6
pitch of vias	P	0.9

IET Microw. Antennas Propag., 2015, Vol. 9, Iss. 15, pp. 1793–1802

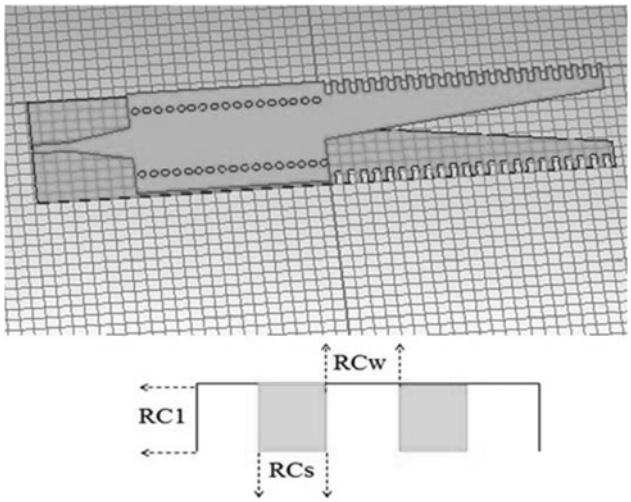

Fig. 2 *Proposed ALTSA with corrugation*

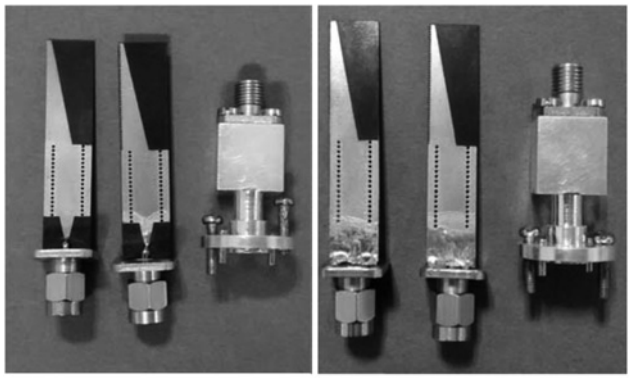

Fig. 3 *Photographs of plain ALTSA and corrugated ALTSA*

a Upper side
b Lower side

[14] is calculated based on (3)

$$W_s = W_{SIW} - 1.08\frac{D^2}{P} + 0.1\frac{D^2}{W_{SIW}} \quad (3)$$

where D is the diameter of the via, P is the space between the vias and W_{SIW} is the SIW width. D and P should be measured precisely to ensure loss free radiation between the metallic vias because of diffraction. Following (4) and (5) allows us to do the same [15] where λ_g is the guided wavelength:

$$D \leq \lambda_g/5 \quad (4)$$

and

$$P \leq 2D \quad (5)$$

2.1 Corrugation structures

Corrugations are well known in the design of horn antennas in order to suppress the higher modes. Therefore, they guarantee the polarisation pureness of antenna [10]. On small antennas, undesired surface current on the outline leads to near-field radiation and thereby leads to reduced gain as well as high SLLs [19, 20]. A planar corrugated surface of exactly quarter wavelength resonant depth, blocks the propagation of an oblique plane wave whose wave vector is perpendicular to the corrugation independently from the direction of the electric field, thus helping them to minimise the radiation toward the undesired direction [21]. Outer rectangular corrugation (RC) structures are applied to the ALTSA design. Fig. 2 shows the ALTSA with outer rectangular corrugation structure. The length and the width are selected to be 1.25 mm (RC_l) and 0.5 mm (RC_w), respectively, with 0.5 mm spacing (RC_s) between the rectangular corrugations, made on the outer edges of the ALTSA [19, 20].

3 Observation and results

Owing to high frequency and smaller wavelength, it is observed that a high number of meshes are needed to accurately model the ALTSA structure and to compute the EM response. Computational EMs (CEMs) models the relation of EM field with physical entities and their environment to evaluate the numerical approximation of Maxwell's equation [19]. CST MWS [22] is based on finite difference time-domain method, which is a popular CEM technique that solves the subset of Maxwell's equations in time domain. Comparison of results using another EM tool ANSYS high-frequency structure simulator based on finite element method, which solves in the frequency domain and obtains a phasor representation of the steady-state finite element field solution has been made for accuracy and simulation time [23].

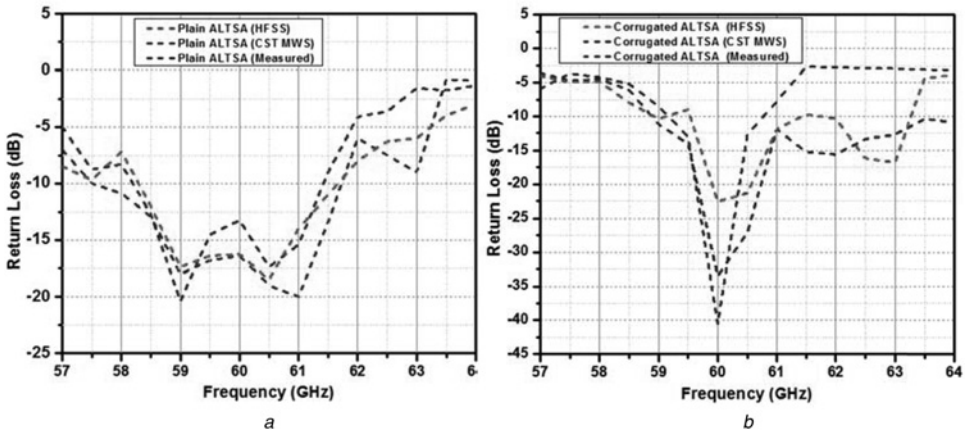

Fig. 4 *Simulated and measured return LoS*

a Plain ALTSA
b Corrugated ALTSA

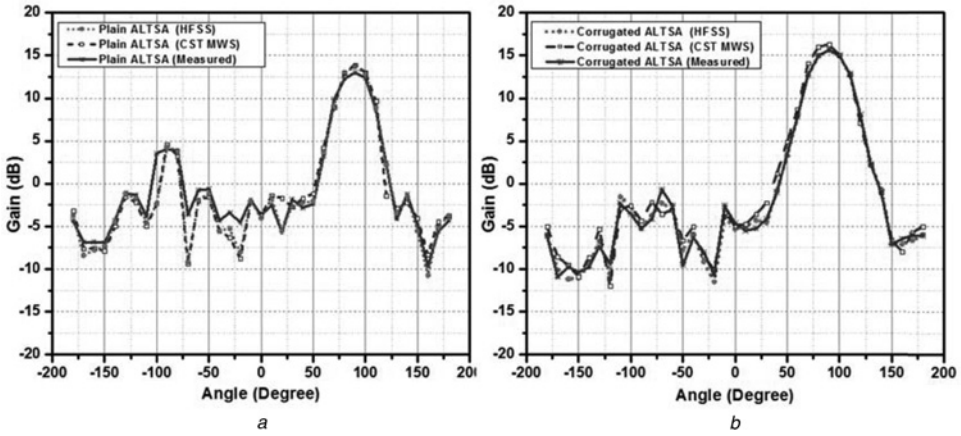

Fig. 5 *Simulated and measured gain*

a Plain ALTSA
b Corrugated ALTSA

Figs. 3*a* and *b* shows the fabricated plain and corrugated ALTSA with waveguide adapter. The measurements were carried out in sub-MmW Laboratory at The Research Center Imarat (RCI), Hyderabad, India. To measure the return loss of the antenna, vector network analyser (VNA) AB MmW's – MVNA-8-350 is calibrated in single port to test the return loss at 60 GHz. To

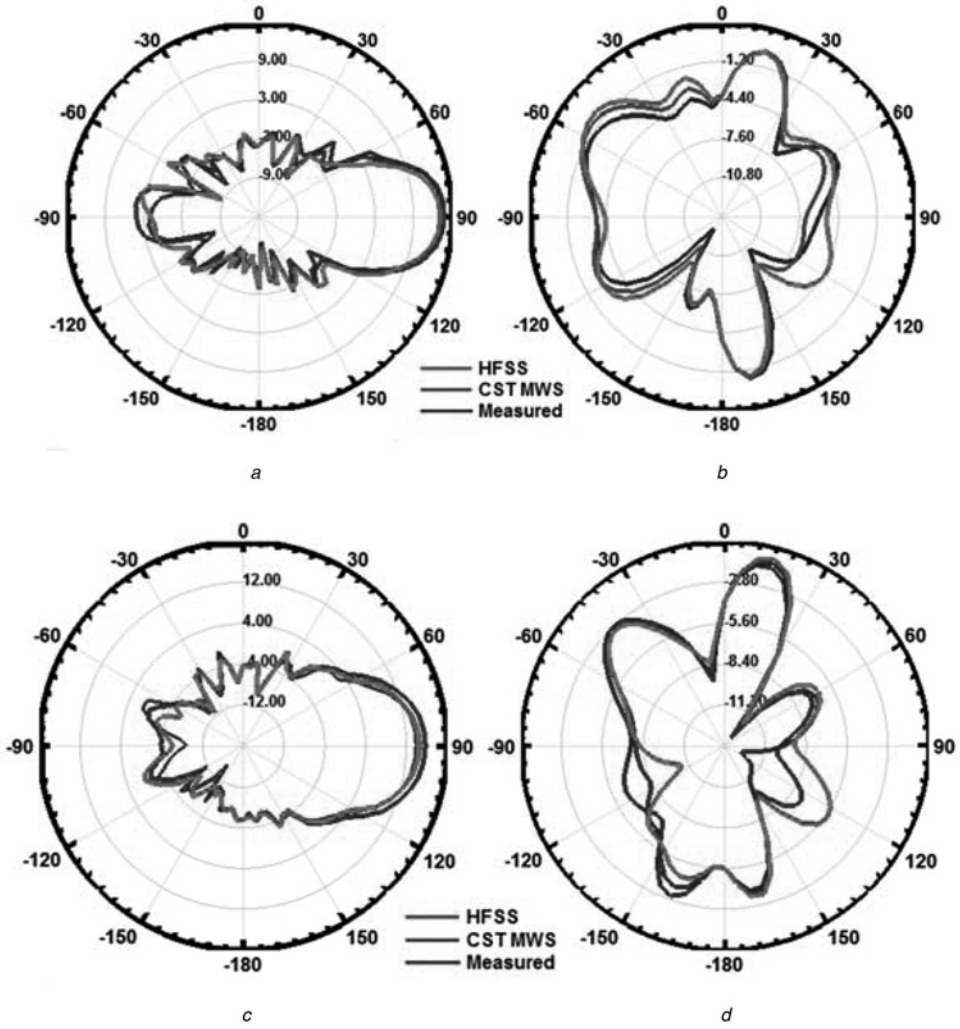

Fig. 6 *Simulated and measured E and H Plane radiation patterns*

a *E*-plane of plain ALTSA
b *H*-plane of plain ALTSA
c *E*-plane of corrugated ALTSA
d *H*-plane of corrugated ALTSA

IET Microw. Antennas Propag., 2015, Vol. 9, Iss. 15, pp. 1793–1802

record the radiation pattern, the VNA is calibrated in two port mode. The separation between the antennas is maintained to be greater than the far-field requirement. The antenna patterns in *E*-plane and *H*-plane were observed.

The impedance match between the ALTSA and SIW is accomplished with the microstrip tapered transition. In [19], subminiature version A (SMA) is used to connect ALTSA to the transceiver. In the present work, waveguide adapter WR-51 to SMA connector has been used to improve the calibration related tolerance range and performance of the antenna. Figs. 4*a* and *b* depict the improved return loss for plain and corrugated ALTSA compared with [19]. The observed return loss for corrugated ALTSA is −41.6 at 60 GHz and the bandwidth of the antenna is 1.5 GHz. Figs. 5*a* and *b* illustrate the simulated and measured gain. The gain and F/B ratio obtained are 13.7 and 11.5 dB for plain ALTSA and 16.5 and 20.83 dB for corrugated ALTSA. Figs. 6*a–d* depict *E* and *H* plane radiation patterns of plain and corrugated ALTSA. Cross *E* and *H* planes of plain and corrugated ALTSA are shown in Figs. 7*a–d*. It is noted that the main lobe direction is along the boresight (*y*-axis). This is important, since MmW applications need a good stability of radiation pattern and directivity. The 3 dB beamwidth for plain ALTSA and corrugated ALTSA is within the range of $32 \simeq 36^{\circ}$, whereas the SLL is between −4 and −9 dB. Simulated and measured results indicate that the corrugation on outer edges of ALTSA contributes more power distribution in the middle of antenna, hence providing the significant impact on the return loss, radiation pattern and the antenna gain. The radiation efficiency of plain ALTSA and corrugated ALTSA are 96.7 and 96.84%, respectively. The performance summary and comparison of the proposed corrugated ALTSA with other similar works available in the literature are shown in Table 2.

4 Channel measurement

Radio wave propagates from the transmitter to receiver in several different ways. In addition to line of sight (LoS) or direct free-space propagation, the waves can reflect, scatter and diffract from objects or propagates through them in some cases. Owing to the shorter wavelength, the propagation loss through the objects in indoor environment is usually very high at MmW frequencies [26]. The radio wave propagation measurements provide information on the propagation channel environment and they are an essential part of the radio system design work. The measured propagation data can be used for implementing realistic channel models and for evaluating antenna in a realistic user environment.

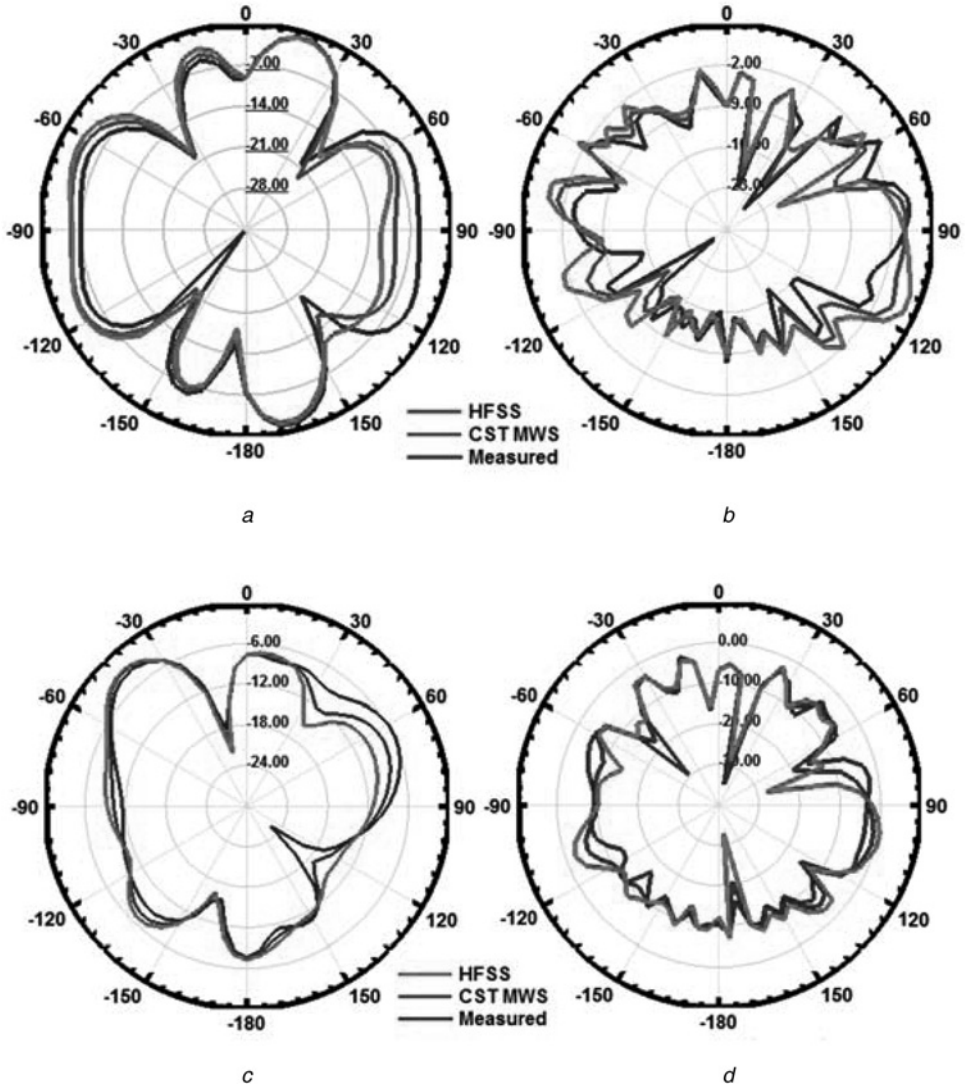

Fig. 7 *Simulated and measured E and H cross-polarisation*

a Cross-*E* of plain ALTSA
b Cross-*H* of plain ALTSA
c Cross-*E* of corrugated ALTSA
d Cross-*H* of corrugated ALTSA

Table 2 Performance summary and comparison of the proposed ALTSA with other similar work available in the literature

References	Frequency, GHz	Size, mm	Gain, dB	Beamwidth, deg
proposed ALTSA	60	22.35	16.5	34.6
[11] (2012)	28	25.6	12.2	48
[8] (2013)	41–61	45	13.5 ≃ 14.9	33 ≃ 36
[24] (2013)	35	27.1	14.5	15
[25] (2014)	50–70	17.5	14.7 ± 0.5	25

To analyse the temporal and spatial variations of a channel, the channel impulse response $h(t)$, between the transmit and receive antennas is a prerequisite. The impulse response provides a linear system perspective but it also encompasses information regarding the nature of propagation delays and the PL associated with all the multipath components. The channel impulse response can be expressed as [27]

$$h(t) = \sum_{k=0}^{N} \alpha_k \delta(t - \tau_k)\, e^{j\theta_k} \tag{6}$$

where N is the number of the detected multipath, $\delta(.)$ is the Dirac delta function, α_k is the multipath gain coefficient of the k_{th} component and τ_k is time varying delay.

5 Test bench and experimental setup

Measurements were carried out in the hallway located on the 13th floor of Tech Park building of SRM University, Chennai, India [global positioning system (GPS) Coordinates: 12° 49′ 29.35″N, 80° 02′ 42.88″E]. Narrow Hallway Environment holds the following dimensions, 14 m length, 1.83 m width and 3 m height, in a modern multi-storied building. The left and right walls of the narrow hallway are made of concrete (relative permittivity $\epsilon_r = 7$) with glass windows ($\epsilon_r = 4$). The floor is covered with porcelain tiles ($\epsilon_r = 6$) and the concrete ceiling is covered with gypsum board ($\epsilon_r = 3$). The same environment with the exact dimensions is approximated in the Wireless InSite to obtain the channel response. Fig. 8*a* depicts the 3D design of narrow hallway environment in Wireless InSite. The photographs of hallway along with measurement setup are shown in Figs. 8*b* and *c*.

The transceiver pair (model:-TRA-5960FW) [28] with corrugated ALTSA antenna was used to carry out the measurements in the narrow hallway environment. To generate 60 GHz frequency, a reference signal of 10 MHz for phase-locked loop and an intermediate frequency of 3 GHz were fed to the transmitter. Power was fed to the transmitter through a signal generator (Agilent's N5182A MXG) [29]. The receiver was connected to the spectrum analyser (Agilent's N9010A EXA) [30] with the span set to 50. The control and data storage were also accomplished by the spectrum analyser. The transmitter and receiver antenna were mounted on a controllable positioning device at the height of 1 m. By the help of this positioner, the antenna could be moved accurately over a certain distance on a linear track during the

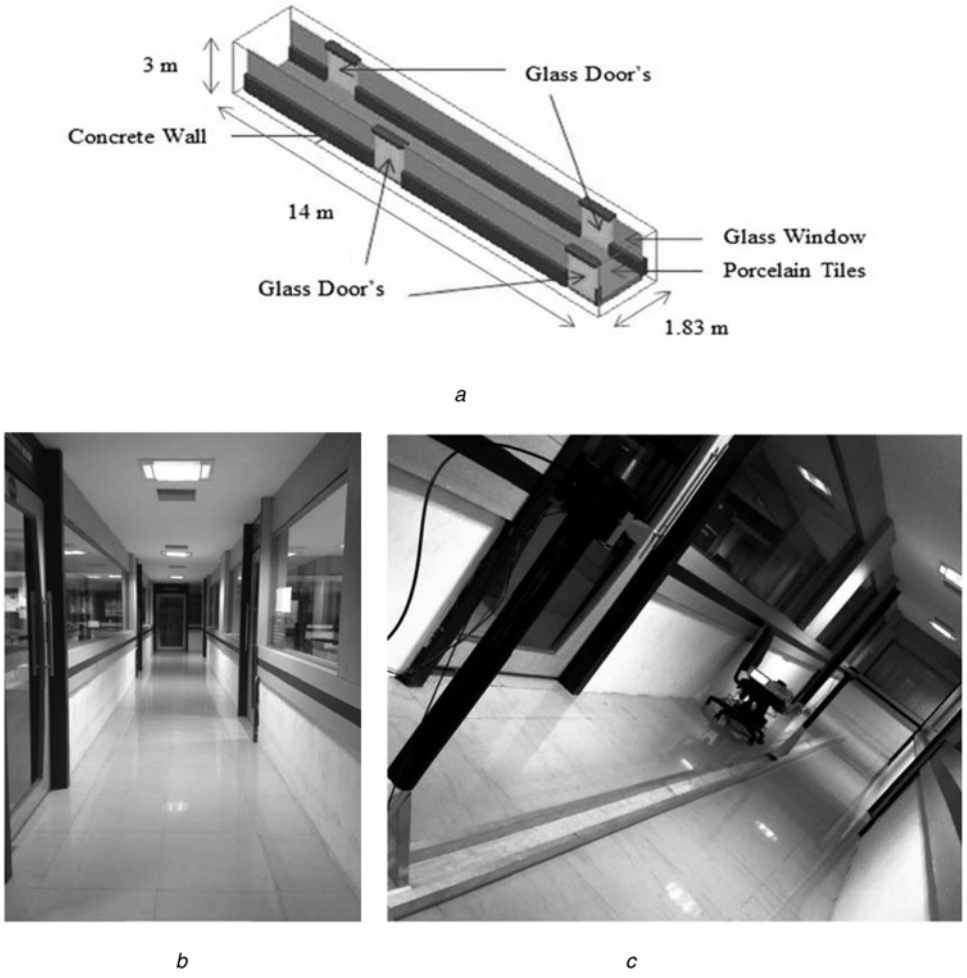

Fig. 8 *Narrow hallway environment*

a 3D design of narrow hallway in Wireless InSite
b Photograph of narrow hallway located on the 13th floor of Tech Park building of SRM University, Chennai
c Photograph of narrow hallway along with measurement setup

IET Microw. Antennas Propag., 2015, Vol. 9, Iss. 15, pp. 1793–1802

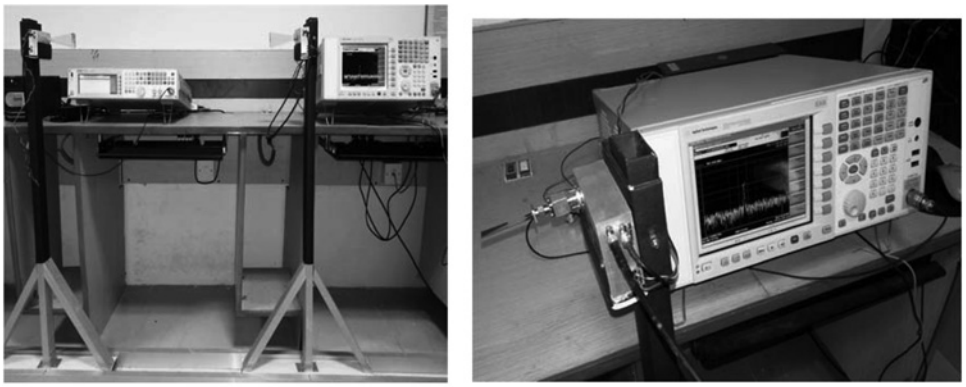

a b

Fig. 9 *Photographs of measurement setup*

a With reference horn antenna
b With corrugated ALTSA

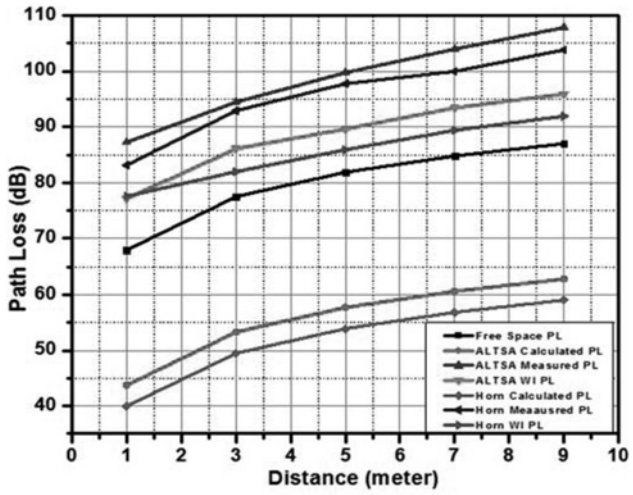

Fig. 10 *Path loss in narrow hallway environment*

measuring procedure. During the acquisition the receiver antenna was moved over a distance of 10 m. Photographs of measurement setup with reference horn antenna and with corrugated ALTSA are shown in Figs. 9*a* and *b*.

6 Result analysis

6.1 Path loss

Radio system design and optimisation require information on the received power for the link budget calculations and the delay dispersion properties of the radio channel. The large-scale fading can be categorised by PL and shadowing. It has distance dependent behaviour, which defines the attenuation of the median power with respect to distance. The value of the received power obtained from measurements is converted into PL. The PL at a distance d from the transmitter is [31]

$$R_{\mathrm{p}}(\mathrm{dBm}) = T_{\mathrm{p}}(\mathrm{dBm}) - \mathrm{PL}(\mathrm{dB}) + G_{\mathrm{T}}(\mathrm{dB}) + G_{\mathrm{R}}(\mathrm{dB}) \quad (7)$$

where T_{P} is the transmitted power in decibel milliwatt (dBm), PL is the path loss in decibels for the transmitter–receiver separation at distance d, R_{P} is the received power measured in dBm, G_{T} is the transmit antenna gain in decibels and G_{R} is the receive antenna gain in decibels. PL exponent n can be derived from the calculated value of PL. The n is given by [27, 31, 32]

$$\mathrm{PL}(\mathrm{dB}) = \mathrm{PL}_{d_0}(\mathrm{dB}) + 10n \log\left(\frac{d}{d_0}\right) + X_\sigma \quad (8)$$

where n is the PL exponent, d_0 is the reference distance at the transmitter which is 1 m in this case, PL_{d_0} is the PL at reference distance d_0, d is the distance between the transmitter and receiver in metres, PL represents the PL at a distance d and X_σ is the Gaussian random variable whose average value is zero and standard deviation is σ. This parameter shows that the PL at any given point will deviate from its average value. From the results, it is observed that the PL for narrow hallway environment increases as the transmitter–receiver separation distance increases. It is observed that the PL varies from 80 to 100 dB in a narrow hallway within an operating space of 10 m. The PL exponent n is 0.95. PL values in free space is much lower as compared with that of the measured values because of several obstructions that practically exists in the propagation path in measurements but does not exist in free space. Fig. 10 depicts the PL value in narrow hallway. For the comparison, the calculated, simulated and

Table 3 Summary of PL in narrow hallway environment

	Path loss, dB						
		ALTSA			Horn		
Distance, m	Free space	Calculated	Wireless InSite	Measured	Calculated	Wireless InSite	Measured
1	67.9	43.7	77.13	87.23	39.94	77.55	83.14
3	77.5	53.3	86.08	94.45	49.48	81.99	92.9
5	81.9	57.7	89.62	99.74	53.92	85.902	97.74
7	84.8	60.6	93.41	103.98	56.84	89.4	99.98
9	87	62.8	95.93	107.84	59.03	91.93	103.84

Table 4 Summary of RMS DS in narrow hallway environment

	RMS DS, ns			
	Horn		ALTSA	
Distance, m	Wireless InSite	Measured	Wireless InSite	Measured
1	0.137	0.152	0.179	0.192
3	0.327	0.455	0.435	0.547
5	0.693	0.754	0.879	0.948
7	0.928	1.048	1.118	1.311
9	1.025	1.332	1.359	1.664

measured PL values for LoS scenario using corrugated ALTSA and horn antenna are given in Table 3.

6.2 Temporal dispersion results

It is not only enough to know the received power of the signal but also the delay and angular dispersions of the propagation channels are of interest for the radio system designers. In a wireless system, the signal received is a summation of several multipath components [33]. The power delay profile (PDP) shows temporal distribution of the power relative to the arriving components [33–37] which are usually calculated in terms of the mean excess delay and the root mean square delay spread (RMS DS). The mean excess delay, τ_m, is defined as the first instant of the PDP [27]

$$\tau_m = \frac{\sum_k p(\tau_k)\tau_k}{\sum_k p(\tau_k)} \tag{9}$$

where τ_k and p are the arrival time and power of the kth path, respectively

$$\tau_{RMS} = \sqrt{\tau_m^2 - (\tau_m)^2} \tag{10}$$

The RMS DS is the square root of the second central instant of the PDP [27]

$$\tau_m^2 = \frac{\sum_k p(\tau_k)\tau_k^2}{\sum_k p(\tau_k)} \tag{11}$$

When compared with the lower frequencies, channel dispersion is smaller in MmW frequencies because echo paths are shorter on average. The RMS DS values obtained is given in Table 4. Table 5 summarises the RMS DS values from the similar research work. The RMS DS values reported by each author vary a great deal. This can be attributed to the complex nature of the 60 GHz channel and the diverse range of propagation scenarios confronting each researcher. It is observed that the use of omnidirectional antenna results in higher RMS DS as compared with directional antenna. When the linear polarisation is used, RMS DS of the channel may range from a few to 100 nanoseconds (ns). It is expected to be higher if omnidirectional antennas are used in large reflective indoor environments. With the high gain antennas, the RMS DS may be limited to a few ns only but this is the case only when the antennas are exactly pointed toward each other. Fig. 11 depicts the RMS DS values in narrow hallway environment.

Table 5 RMS DS in different indoor environments in the 60 GHz frequency range. The measurements have been performed in LoS environments

Environment	RMS DS, ns	Transmitting antenna	Receiving antenna	References
aircraft cabin	2.2	horn	horn	[36]
private home	3	omni	omni	[37]
conference room	4.7	omni	horn	[38]
office	9	horn	omni	[39]
laboratory room	13.6	horn	omni	[37]
corridor	3.4	horn	omni	[37]
hall	13.4	omni	omni	[40]

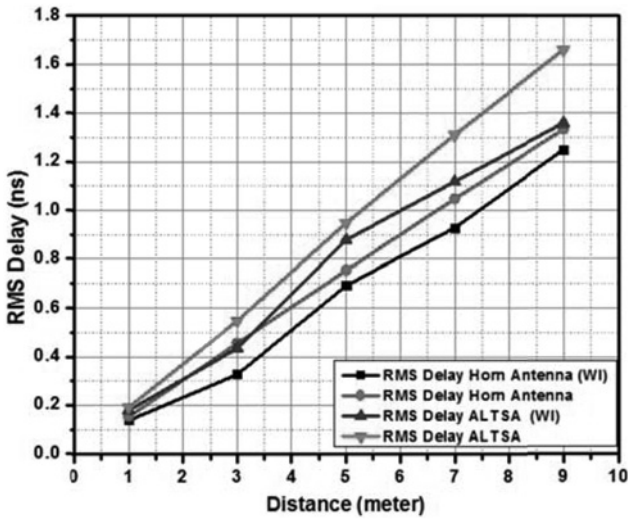

Fig. 11 *RMS DS in narrow hallway environment*

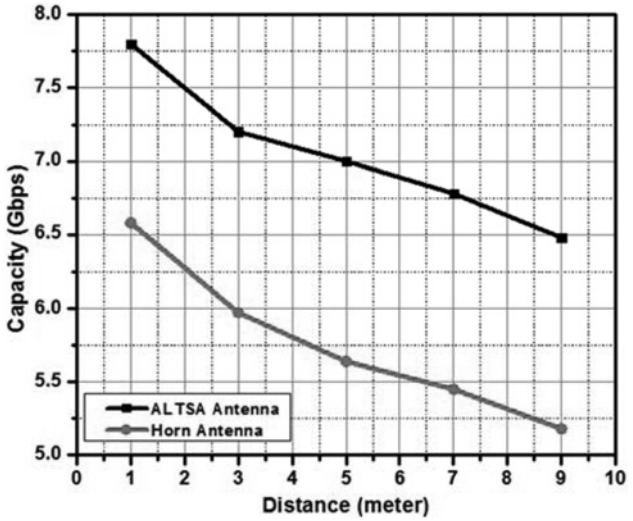

Fig. 12 *Maximum achievable capacity value in narrow hallway environment*

6.3 Capacity estimation

Further effort was made to determine the capacity, the maximum rate at which information can be transmitted. As 60 GHz has the potential to provide the multi-gigabit data rates, it can be used for high definition multimedia transmissions. The channel capacity (C) defines the maximum achievable throughput in the specified channel condition. Capacity is set by the bandwidth and signals to noise ratio and can be given as [41–43]

$$C = W * \log_2\left(\frac{E_b}{N_0} + 1\right) \tag{12}$$

where W is the available bandwidth of the system and (E_b/N_0) is a measure of the signal strength relative to the background noise and

Table 6 Summary of capacity value in narrow hallway environment

	Shannon capacity, bits/s	
Distance, m	ALTSA	Horn
1	7.8×10^9	6.5×10^9
3	7.2×10^9	5.9×10^9
5	7×10^9	5.6×10^9
7	6.7×10^9	5.4×10^9
9	6.4×10^9	5.1×10^9

can be obtained by [40, 41]

$$\frac{E_b}{N_0} = R_p - 10\log(KT_{syst}) - 10\log(W) - NF_{RX} \quad (13)$$

where R_p is the received power, 10 log (kT_{syst}) is equal to 174 dBm/Hz for a system temperature of 17°C, NF_{RX} is the noise figure of the receiver in decibels and W is the bandwidth of the signal in hertz. The receiver noise figure is assumed to be 6 dB [40, 41] and the RF bandwidth is assumed to be 1.5 GHz. Fig. 12 shows the maximum achievable capacity value in a narrow hallway environment. It is observed that the capacity decreases with increasing distance. The horn antenna bandwidth of 1.25 GHz gives the maximum data rate of 6.5 Gbps and with 1.5 GHz bandwidth of corrugated ALTSA the maximum data rate increases up to 7.8 Gbps. Table 6 provides the summary of capacity value in narrow hallway environment.

7 Conclusions

In this research work, ALTSA with outer rectangular corrugations using SIW feed is designed for 60 GHz wireless communications. The proposed antenna has high gain of 16.5 dB and a bandwidth of 1.5 GHz. To substantiate the antenna design at 60 GHz for WLAN and WPAN applications, large-scale and small-scale indoor radio link characterisation has been made in a narrow hallway environment utilising RF experiments. From our results, we observed that the antenna radiation pattern has a significant effect on the received power. ALTSA has a good power performance because of its bandwidth and radiation pattern. Furthermore, the architectural design, dimensions and materials used in the vicinity of the transmitter and receiver antennas play a key role for the significant variations in the received signal strength and PDP. It is observed that the PL varies from 80 to 100 dB in a narrow hallway within an operating space of 10 m. It is seen that when the high gain antennas are used, the RMS DS has been limited to a few ns. Furthermore, the performed study shows that the ALTSA has a higher capacity compared with the horn antenna with the maximum capacity of 7.8 Gbps within an operating space of 10 m. The propagation properties of ALTSA at MmW and compact size make it viable to be integrated on the same substrate with other MmW receiver or transmitter components. This makes it a suitable candidate for the ultra-high-speed multimedia applications for WLAN and WPAN. However, due to the complex nature of MmW propagation, there are still a lot of unknowns that need to be quantified. With this in mind, the work presented in this paper serves as a valuable contribution to the deployment of MmW-based WLANs and WPANs which will expect to proliferate in big way in coming years.

8 Acknowledgments

Authors are very much thankful to The Defence Research and Development Organisation (DRDO), Government of India, for providing necessary support to carry out this research work.

9 References

1 Yong, S.K., Xia, P., Garcia, A.V.: '60 GHz Technology for Gbps WLAN and WPAN: from theory to practice' (John Wiley and Sons Ltd., Chichester, UK, 2011, 1st edn.)
2 Rappaport, T.S., Murdock, J.N., Gutierrez, F.: 'State of the art in 60 GHz integrated circuits and systems for wireless communications', *Proc. IEEE*, 2011, **99**, (8), pp. 1390–1436
3 Smulders, P.: 'Exploiting the 60 GHz band for local wireless multimedia access: prospects and future directions', *IEEE Commun. Mag.*, 2002, **40**, (1), pp. 140–147
4 Huang, K.C., Edwards, D.J.: 'Millimetre wave antennas for gigabit wireless communications: a practical guide to design and analysis in a system context' (John Wiley and Sons Ltd., Chichester, UK, 2008, 1st edn.)
5 Rodenbeck, C.T., Kim, S.G., Tu, W.H., *et al.*: 'Ultrawideband low cost phased array radars', *IEEE Trans. Microw. Theory Tech.*, 2005, **53**, (12), pp. 3697–3703
6 Namas, T., Hasanovic, M.: 'Ultrawideband antipodal vivaldi antenna for road surface scanner based on inverse scattering'. Proc. 28th Annual Review of Progress in Applied Computational Electromagnetics, Colombus, OH, USA, April 2012, pp. 882–887
7 Coburn, W.K., Zaghloul, A.I.: 'Numerical analysis of stacked tapered slot antennas'. Proc. 28th Annual Review Progress in Applied Computational Electromagnetics, Colombus, OH, USA, April 2012, pp. 112–117
8 Taringou, F., Dousset, D., Bornemann, J., *et al.*: 'Broadband CPW feed for millimeter-wave SIW-based antipodal linearly tapered slot antennas', *IEEE Trans. Antennas Propag.*, 2013, **61**, (4), pp. 1756–1762
9 Hao, Z.C., Hong, W., Chen, J., *et al.*: 'A novel feeding technique for antipodal linearly tapered slot antenna array'. Proc. IEEE Int. Microwave Symp. Digest, China, June 2005, vol. 3, pp. 1641–1643
10 Sugawara, S., Maita, Y., Adachi, K., *et al.*: 'Characteristics of a Mm-wave tapered slot antenna with corrugated edges'. Proc. IEEE Int. Microwave Symp. Digest, Baltimore, USA, June 1998, vol. 2, pp. 533–536
11 Djerafi, T., Wu, K.: 'Corrugated substrate integrated waveguide (SIW) antipodal linearly tapered slot antenna array fed by quasi-triangular power divider', *Prog. Electromagn. Res. C*, 2012, **26**, pp. 139–151
12 Bozzi, M., Perregrini, L., Wu, K., *et al.*: 'Current and future research trends in substrate integrated waveguide technology', *Radioengineering*, 2009, **18**, (2), pp. 201–209
13 Wood, I., Dousset, D., Bornemann, J., *et al.*: 'Linear tapered slot antenna with substrate integrated waveguide feed'. Proc. IEEE Int. Symp. Antennas Propagation Society, Honolulu, Hawaii, June 2007, pp. 4761–4764
14 Huang, T.J., Heng, T.H.: 'Antipodal dual exponentially tapered slot antenna (DETSA) with stepped edge corrugations for front-to-back ratio improvement'. Proc. IEEE Asia Pacific Microwave Conf., Melbourne, Australia, December 2011, pp. 685–688
15 Yoon, D.G., Hong, Y.P., An, Y.J., *et al.*: 'High-gain planar tapered slot antenna for ku-band applications'. Proc. IEEE Asia Pacific Microwave Conf., Yokohama, Japan, December 2010, pp. 1914–1917
16 Yang, L.L.: '60 GHz: opportunity for gigabit WPAN and WLAN convergence', *ACM SIGCOMM Comput. Commun. Rev.*, 2009, **39**, (1), pp. 56–61
17 Jiang, C.: 'Microwave and millimeter-wave integrated circuit systems in packaging'. PhD thesis, DTU Electrical Engineering, Technical University of Denmark, 2010
18 Ellis, T.J., Rebeiz, G.M.: 'MM-wave tapered slot antennas on micromachined photonic bandgap dielectrics'. Proc. IEEE MTT-S Int. Microwave Symp. Digest, San Francisco, USA, June 1996, vol. 2, pp. 1157–1160
19 Shrivastava, P., Chandra, D., Tiwari, N., *et al.*: 'Investigations on corrugation issues in SIW based antipodal linear tapered slot antenna for wireless networks at 60 GHz', *Appl. Comput. Electromagn. Soc. J.*, 2013, **28**, (10), pp. 960–968
20 Rao, T.R., Shrivastava, P., Tiwari, N.: 'Investigations of corrugation issues in SIW based antipodal linear tapered slot antenna at 60 GHz'. Proc. European Conf. Antennas and Propagation, Gothenburg, Sweden, April 2013, pp. 2104–2107
21 Scappuzzo, F.S., Makarov, S.N.: 'A low-multipath wideband GPS antenna with cutoff or non-cutoff corrugated ground plane', *IEEE Trans. Antennas Propag.*, 2009, **57**, (1), pp. 33–46
22 'CST MICROWAVE STUDIO'. Available at https://www.cst.com/Products/CSTMWS/Performance
23 'Ansys HFSS Technical Notes'. Available at http://www.ansys.com/Products/Simulation+Technology/Electronics/Signal+Integrity/ANSYS+HFSS
24 Wang, W., Wang, X., Wang, W., *et al.*: 'Planar high-gain antipodal linearly tapered slot antenna for passive millimeter-wave focal plane array imaging'. Proc. IEEE Int. Symp. Phased Array Systems & Technology, Waltham, MA, USA, October 2013, pp. 267–271
25 Ismail, M., Sebak, A.R.: 'High-gain SIW-based antipodal linearly tapered slot antenna for 60 GHz applications'. Proc. IEEE Antennas and Propagation Society Int. Symp., Memphis, TN, USA, June 2014, pp. 217–218
26 Cabric, D., Chen, M.S.W., Sobel, D.A., *et al.*: 'Future wireless systems: UWB, 60 GHz, and cognitive radios'. Proc. IEEE Conf. Custom Integrated Circuits, San Jose, CA, USA, September 2005, pp. 793–796
27 Rappaport, T.S.: 'Wireless communications: principles and practice' (Prentice-Hall PTR, NJ, 1996)
28 Yang, K.S., Choi, S.T., Nishi, S., *et al.*: '60 GHz High integrated transceiver for broad band short distance communication'. Proc. URSI General Assemblies, New Delhi, India, October 2005
29 'MXG Vector Signal Generator'. Available at http://www.keysight.com/en/pd-797248-pn-N5182A/mxg-rf-vector-signal-generator?&cc=IN&lc=eng

30 'EXA X-Series Signal Analyzer'. Available at http://www.cp.literature.agilent.com/litweb/pdf/5989-6529EN.pdf
31 Jung, M.W., Kim, J., Yoon, Y.K.: 'Measurements of path loss in MM-wave for indoor environments'. Proc. IEEE Asia Pacific Microwave Conf., Singapore, December 2009, pp. 1068–1071
32 Wei, F., Jun, H., Shuhan, Z.: 'Frequency-domain measurement of 60 GHz indoor channels: a measurement setup, literature data, and analysis', *IEEE Instrum. Meas. Mag.*, 2013, **16**, (2), pp. 34–40
33 Moraitis, N., Constantinou, P.: 'Indoor channel measurements and characterization at 60 GHz for wireless local area network applications', *IEEE Tran. Antennas Propag.*, 2004, **52**, (12), pp. 3180–3189
34 Gustafson, C., Haneda, K., Wyne, S., *et al.*: 'On Mm-wave multipath clustering and channel modeling', *IEEE Trans. Antennas Propag.*, 2014, **62**, (3), pp. 1445–1455
35 Talbi, L., LeBel, J.: 'Broadband 60 GHz sounder for propagation channel measurements over short/medium distances', *IEEE Trans. Instrum. Meas.*, 2014, **63**, (2), pp. 343–351
36 Garcia, A.P., Kotterman, W., Trautwein, U., *et al.*: '60 GHz time-variant shadowing characterization within an airbus 340'. Proc. European Conf. Antennas and Propagation, Barcelona, Spain, April 2010, pp. 1–5
37 Zwick, T., Beukema, T.J., Nam, H.: 'Wideband channel sounder with measurements and model for the 60 GHz indoor radio channel', *IEEE Trans. Veh. Technol.*, 2005, **54**, (4), pp. 1266–1277
38 Manabe, T., Miura, Y., Ihara, T.: 'Effects of antenna directivity and polarization on indoor multipath propagation characteristics at 60 GHz', *IEEE J. Sel. Areas Commun.*, 1996, **14**, (3), pp. 441–448
39 Siamarou, A., Al-Nuaimi, M.: 'Multipath delay spread and signal level measurements for indoor wireless radio channels at 62.4 GHz'. Proc. 53rd IEEE Vehicular Technology Conf., Rhodes, Greece, May 2001, vol. 1, pp. 454–458
40 Geng, S., Kivinen, J., Zhao, X., *et al.*: 'Millimeter-wave propagation channel characterization for short-range wireless communications', *IEEE Trans. Veh. Technol.*, 2009, **58**, (1), pp. 3–13
41 Geng, S.: 'Performance and capacity analysis of 60 GHz WPAN channel', *Microw. Opt. Technol. Lett.*, 2009, **51**, (11), pp. 2671–2675
42 Kumar, A., Rama Rao, T.: 'Analysis of planning and deployment issues for short-range gigabit wireless communications at 60 GHz', *Int. J. Microw. Opt. Technol.*, 2014, **9**, (2), pp. 156–163
43 Rama Rao, T., Murugesan, D., Labay, V.A.: '60 GHz wave propagation studies in an indoor office & corridor environments', *Int. J. Microw. Opt. Technol.*, 2012, **7**, (5), pp. 308–317